Hydrodynamic Characteristics of a Three-Phase Inverse Fluidized-Bed Column

Yasser A. A. Ibrahim, Cedric L. Briens, Argyrios Margaritis, and Maurice A. Bergongnou
Dept. of Chemical and Biochemical Engineering, The University of Western Ontario, London, Ontario, Canada, N6A 5B9

Gas–liquid–solid inverse fluidized beds were studied, in which the gas and the continuous liquid phase flow countercurrently fluidizing particles that are lighter than the liquid. Conductivity and static pressure measurements were combined to provide the vertical profiles of the gas, liquid and solid holdup, in beds of 4- or 6-mm polypropylene particles with a density of about 870 kg/m^3. Various bed heights were obtained with different measurement methods. The minimum fluidization velocity was estimated using the bed static pressure gradient. A new transition velocity, called the uniform fluidization velocity, was identified using conductivity measurements. This is the superficial liquid velocity at which the fluidization quality becomes the same throughout the bed.

Introduction

In classic three-phase fluidization (Fan, 1989), particles of a density larger than the liquid are fluidized by an upward concurrent flow of liquid and gas. The liquid is the continuous phase while the gas bubbles up through the bed. In three-phase inverse fluidization, the particles have a smaller density than the liquid ($\rho_s < \rho_l$), gas flows upward, and liquid flows downward. The liquid is the continuous phase (Fan, 1989). Three-phase inverse fluidization has not yet received much attention. The countercurrent fluidization of light particles with liquid as continuous phase was first recognized in 1970 (Page, 1970). Its application, specially to wastewater treatment, resulted in a patent to Shimodaira et al. (1981). Three-phase inverse fluidization warrants further investigation, as this mode of operation is very promising for wastewater treatment, biochemical, and other industrial applications. In three-phase inverse fluidization, the solids can be fluidized at low liquid velocity, that is, with little energy expenditure, and the solids attrition is minimum. Similar advantages could theoretically be achieved with regular concurrent fluidization of particles with density slightly larger than that of water. However, a slight decrease in particle density caused, for example, by gas evolution would result in considerable particle entrainment. Three-phase inverse fluidization does not present this problem.

Correspondence concerning this article should be addressed to C. L. Briens.

Publications on the hydrodynamic characteristics of two- and three-phase inverse fluidization have addressed the various operating regimes (Chern, 1982; Fan et al., 1982a,b; Chern et al., 1983; Legile et al., 1988). The minor differences between the operating regimes reported in these publications can be attributed to differences in equipment, such as the gas and liquid distributors. Investigation of the bed-expansion characteristics has led to the development of some semiempirical models for two-phase beds (Fan et al., 1982a; Karamanev and Nikolov, 1992) and three-phase beds (Legile et al., 1988). Bed voidage and phase holdups were also measured in a limited number of particle systems (Fan et al., 1982a; Legile et al., 1988). The effect of liquid coalescing properties was only reported in one study, by Thomas and Bernis (1989).

In all of the studies just cited, the expanded bed height was obtained from either visual observations (Legile et al., 1988; Karamanev and Nikolov, 1992), or from the static pressure profile (Fan et al., 1982a; Legile et al., 1988). Visual observations may be suitable when the bed surface fluctuations are moderate, that is, in the absence of gas. Preliminary experiments indicated that they give inaccurate results in three-phase beds at elevated gas velocities. On the other hand, the static pressure profile method requires a significant density difference between the solids and the liquid. Unfortunately, inverse gas–liquid–solid fluidized beds are most attractive

when the densities of the particles and the liquid are close since they are easier to fluidize with a smaller liquid recycle ratio.

The first objective in this article was, therefore to develop an accurate method of measuring the fluidization characteristics of inverse three-phase fluidized beds that could be applied to any kind of particle density. The second objective was to use this new method as well as the static pressure to identify the hydrodynamic regimes and to find the vertical profile of the phase holdups.

Equipment

A 17-cm Altuglass column was used as the inverse fluidization unit. Its total height was 2.5 m, with a 1.7-m-high test section. A retaining stainless steel screen was located just below the fluidized-bed liquid distributor section. This screen prevented the particles from rising from the bed to the top portion of the column. All bed-height measurements were taken relative to the screen level and downward. A diagram of the equipment is shown in Figure 1. Air and an aqueous 5 wt. % sodium chloride solution were the gas and liquid phases.

The flow rate of the air was regulated and measured with a bank of calibrated sonic nozzles. Sonic nozzles provide precise control of the air flow rate that is not affected by downstream pressure fluctuations. The air was saturated with water vapor in a humidification column upstream of the inverse fluidized-bed column. The air was then admitted to the column through a gas sparger with six arms. Each arm had six 0.3-mm-dia. holes. The pressure drop across the sparger was high enough to maintain good gas distribution over the whole range of gas flow rates. The liquid was pumped to the fluidization column where an overflow maintained a constant liquid flow rate by eliminating the effect of pump fluctuations. Good liquid distribution was obtained with the help of a pipe distributor containing 36 holes (5 mm in diameter), and a fluidized-bed section of 6-mm particles with a density of 862 kg/m^3. The liquid flow rate through the column was controlled by a valve (V2 in Figure 1) and the velocity was measured by an elbow meter (EL1 in Figure 1). During preliminary experiments, the maximum flow rates of both gas and liquid were determined by flooding conditions. Flooding was characterized by the formation of a gas pocket under the retaining screen. High gas flow rates were avoided to reduce excessive solids entrainment. All reported gas velocities were for 1 atm, 20°C.

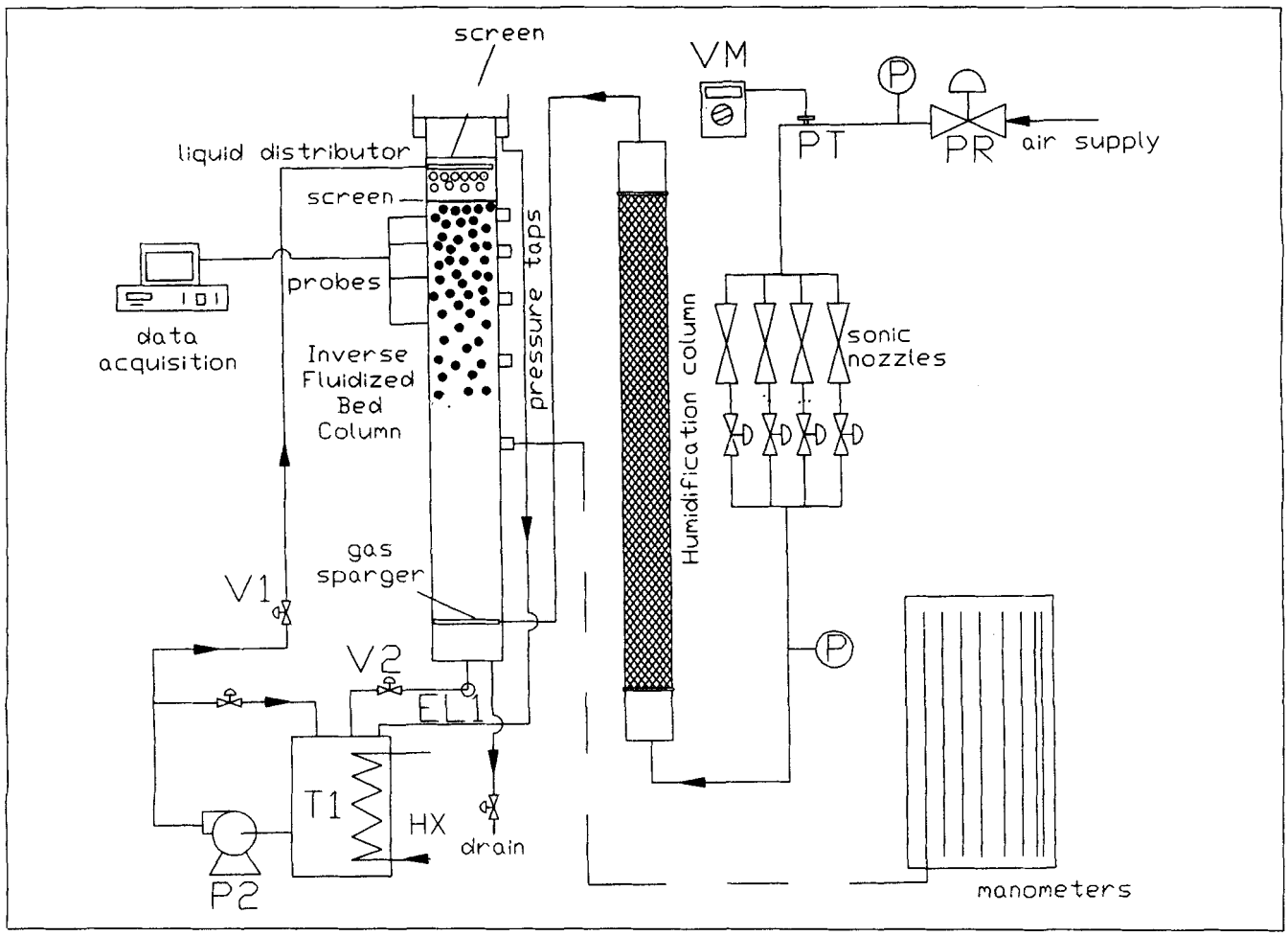

Figure 1. Experimental setup.

EL: elbow meter; HX: heat exchanger; P: pressure gauge; PR: pressure regulator; PT: pressure transducer; T: tank; V: valve; VM: voltmeter.

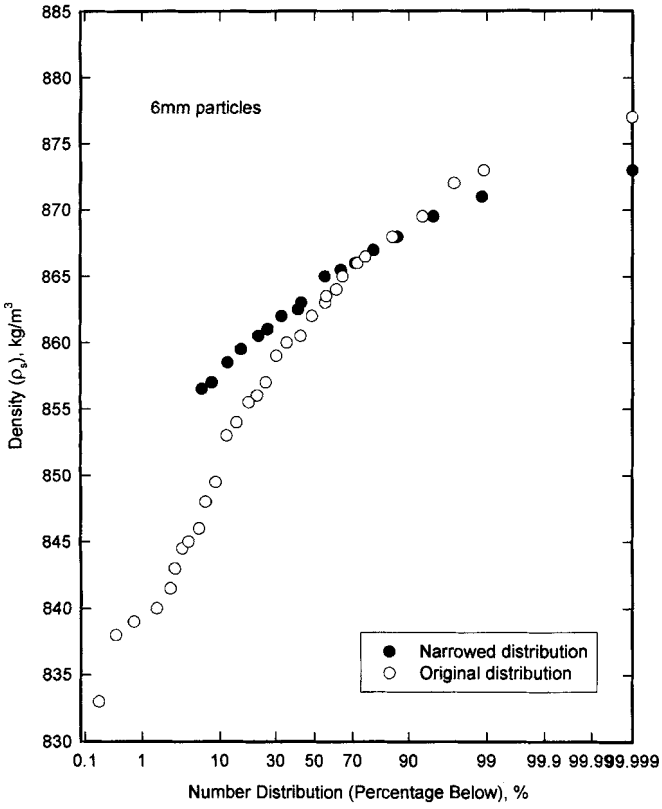

Figure 2. Original and narrowed cumulative density distribution of 6-mm particles.

The liquid temperature was controlled within 0.2°C of 28°C with the heat-exchange coil (HX) in the solution tank T1. This temperature control ensured that the physical properties of the solution remained constant.

Static pressure was measured at the column wall using 22 pressure taps. Each pressure tap was designed to also perform as a conductivity electrode.

Perfectly spherical and hollow polypropylene particles of either 4 or 6 mm in diameter were used as the solid phase. These particles sizes were chosen because they are close to the particle size used for three-phase inverse fluidization in wastewater treatment (Fan, 1989). The density distribution of the particles was measured with a mixture of ethanol and water. The original density distribution was narrowed in order to achieve uniform fluidization. Figure 2 shows the density distribution for the 6-mm particles before and after narrowing the density distribution. The average particle density was 862 kg/m^3 for the 6-mm particles and 877 kg/m^3 for the 4-mm particles.

Conductivity Technique

The new conductivity technique uses 18 sets of noninvasive conductivity electrodes. Each set is made of two stainless steel electrodes at the column wall and at the same horizontal level. The electrodes are simultaneously supplied with a 60-Hz AC current. The conductivity of the gas–liquid–solid mixture between the two electrodes of each set was measured with the help of a data-acquisition system. The sampling frequency was at least 125 Hz per electrode, with a sampling time of 30 s. The instantaneous readings of each electrode were averaged over 30 s to yield a value that is proportional to the conductivity of the mixture in the column. Since both the gas bubbles and the solid particles are nonconductive, this average value of conductivity can be directly related to the liquid holdup, ϵ_l.

The use of the relative conductivity eliminated the effects of minor variations in the electrode characteristics. It is obtained from the ratio of the measured conductance (Γ) at a given condition to the conductance measured with the same electrode in liquid only:

$$\gamma_r = \frac{\gamma}{\gamma_0} = \frac{\Gamma}{\Gamma_0} \tag{1}$$

The same liquid holdup (ϵ_l) should result in the same γ_r independent of which electrode set was used.

Preliminary results of conductivity measurements showed that the liquid holdup cannot be directly related to the relative conductivity (γ_r) as suggested by Begovich and Watson (1978). A calibration was thus performed in the liquid–solid fluidized bed in the absence of gas. The expanded bed height was visually measured for different liquid flow rates. The solid holdup was then obtained from the known mass of solids in the column. The liquid holdup was calculated by difference. The relative conductivity data for each electrode was correlated with the corresponding liquid holdup giving a correlation for all the electrodes:

$$\epsilon_l = (\gamma_r)^{1.27} \tag{2}$$

This correlation and the 18 electrode sets provided the axial profile of the liquid holdup and hence the bed height in less than 5 min.

Discussion

In three-phase inverse fluidization, gas bubbles move up the column countercurrently with the liquid. Figure 3 is a diagram of the bed under various flow conditions. In the presence of gas and at low liquid velocity, most of the bed is fixed, although the lower section of the bed is fluidized, as shown in Figure 3a. As the liquid flow rate is increased, the fluidized bed section grows upward. All the particles start to move freely at the minimum fluidization condition. Past minimum fluidization, although the whole bed was fluidized, the fluidization quality varied with height. As shown in Figure 3b, the bottom part of the bed was less dense than the rest of the bed. Under these conditions, some liquid recirculation currents were observed. As the liquid flow rate was increased further, the bed became homogeneous and liquid recirculation currents disappeared, as shown in Figure 3c.

Minimum liquid fluidization velocity

Minimum fluidization is defined as the condition at which the pressure drop across the bed is equal to the weight of the bed (Fan, 1989). For each gas velocity, the minimum liquid fluidization velocity corresponds to the velocity at which the pressure gradient within the bed is minimum. Therefore, it

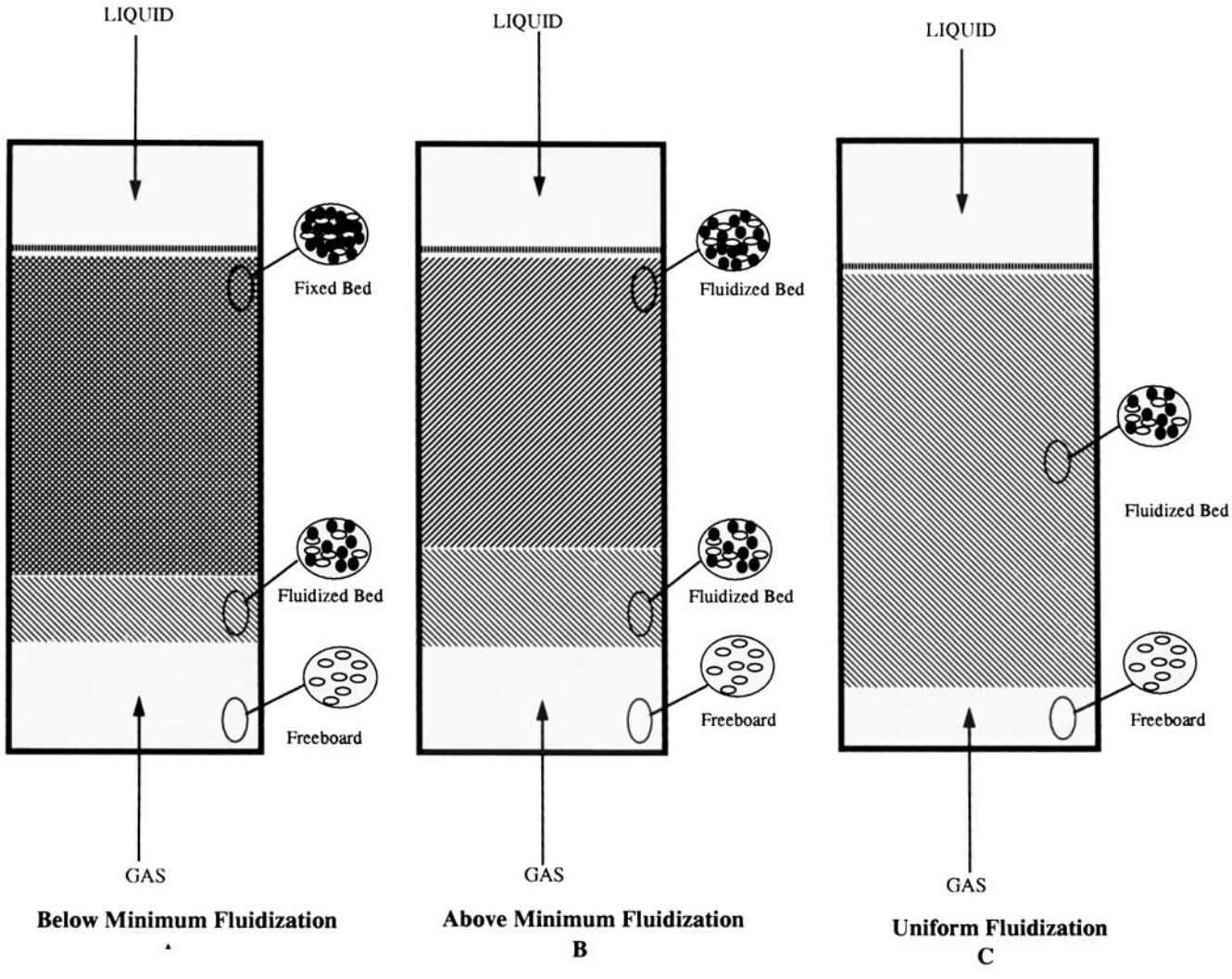

Figure 3. Three-phase inverse fluidized bed under various liquid flow conditions.

was obtained from a plot of the pressure gradient against the liquid velocity at constant gas velocity (Figures 4 and 5). The bed pressure gradient was obtained from the pressure profile as in Figure 6. The same technique is used by most researchers (Legile et al., 1988; Fan, 1989).

Figure 7 shows that the minimum fluidization velocity decreased as the gas velocity was increased. Similar results were obtained by Legile et al. (1988) for two different types of particles, cork and polyethylene. Increasing the gas velocity displaces some of the liquid, resulting in a lower liquid holdup and a larger interstitial liquid velocity (U_l/ϵ_l). The slip velocity between liquid and particles increases and the larger drag exerted on the particles leads to early fluidization.

The conductivity method was also used to find the minimum fluidization velocity as shown in Figure 8. The static bed height was 29.5 cm, which means that the electrode at 29 cm was at the boundary between the bed and the freeboard at liquid velocities smaller than the minimum fluidization velocity. At low velocities, this electrode gave a relative conductivity of about 1, which was not affected by the liquid velocity. Figure 8 shows that the relative conductivity it measured started dropping at a velocity of about 1.2 cm/s. This is slightly higher than the 1.0 cm/s value obtained from static pressure measurements, since the bed must first fluidize and expand to cover the bottom electrode.

When the bed is fully fluidized, the conductivity should be the same for all the electrodes within the bed. Figure 8 shows that this occurs at a velocity of about 1.5 cm/s, while the minimum fluidization velocity obtained from the pressure method was at 1.0 cm/s. This discrepancy led to the concept of uniform fluidization velocity.

Uniform fluidization velocity

While the whole bed was fluidized at velocities greater than the minimum fluidization velocity, hydrodynamics appeared to be different at the top and bottom of the bed. This nonuniform fluidization tended to disappear as the liquid velocity was increased to about 1.5 cm/s, the value at which the relative conductivity of all the electrodes within the bed will become almost the same (see Figure 8). This transition velocity, at which the fluidization becomes uniform, appeared to be independent of the distributor design. It is termed the *uniform fluidization velocity*, U_{luf}. This definition implies that,

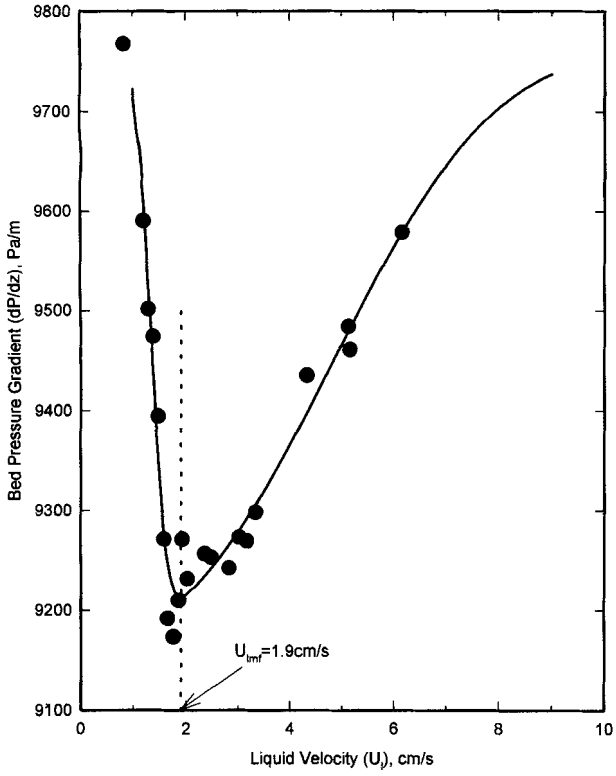

Figure 4. Bed pressure gradient (dP/dz) vs. liquid velocity (U_{lmf}) for 6-mm particles in liquid solid system.

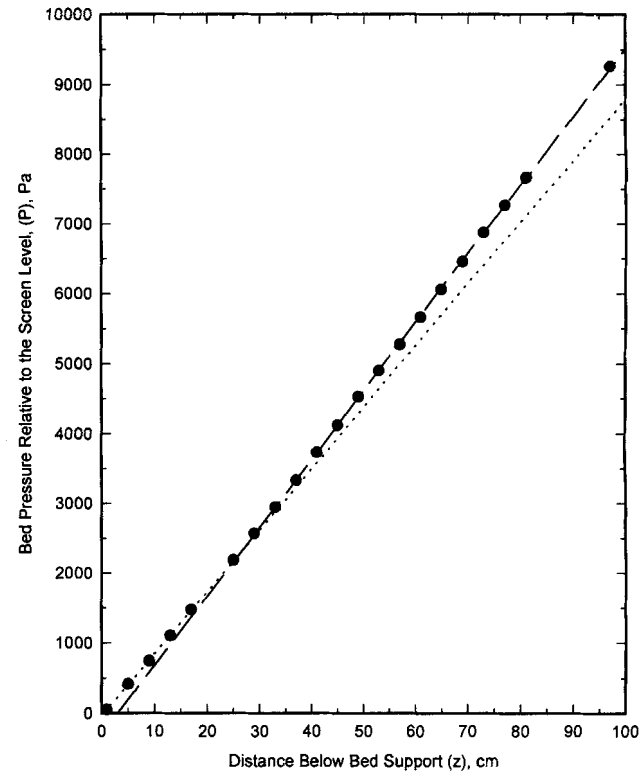

Figure 6. Typical pressure profile for three-phase inverse fluidized bed.

U_g = 0.35 cm/s, U_l = 0.9 cm/s, 4-mm particles.

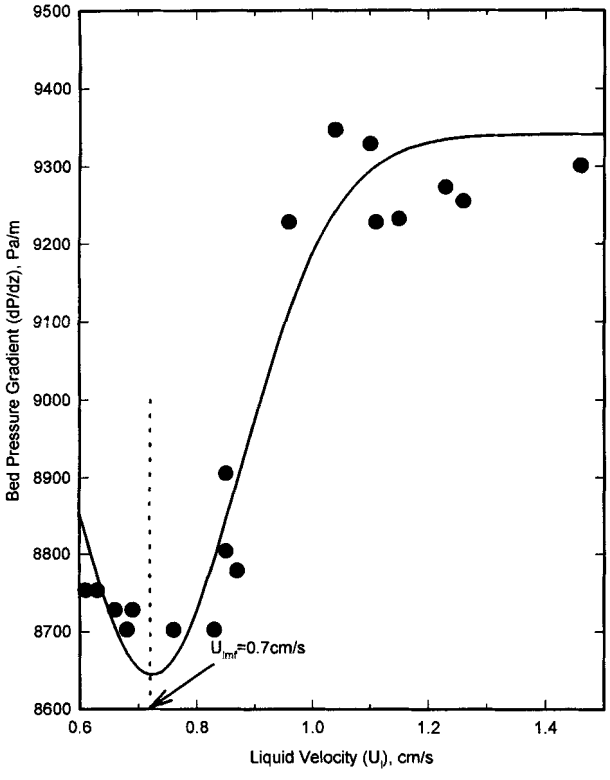

Figure 5. Bed pressure gradient (dP/dz) vs. liquid velocity (U_{lmf}) for 4-mm particles in gas liquid solid system (U_g = 0.39 cm/s).

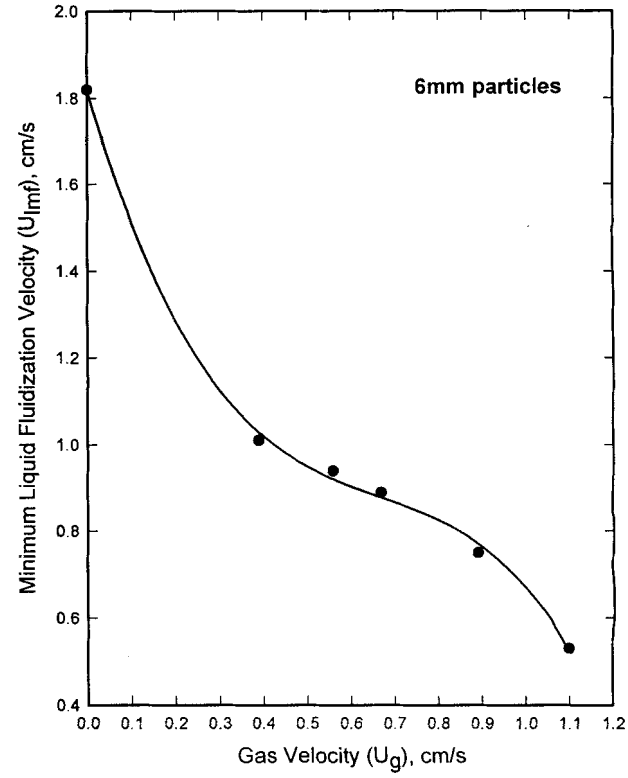

Figure 7. Minimum liquid fluidization velocity vs. gas velocity.

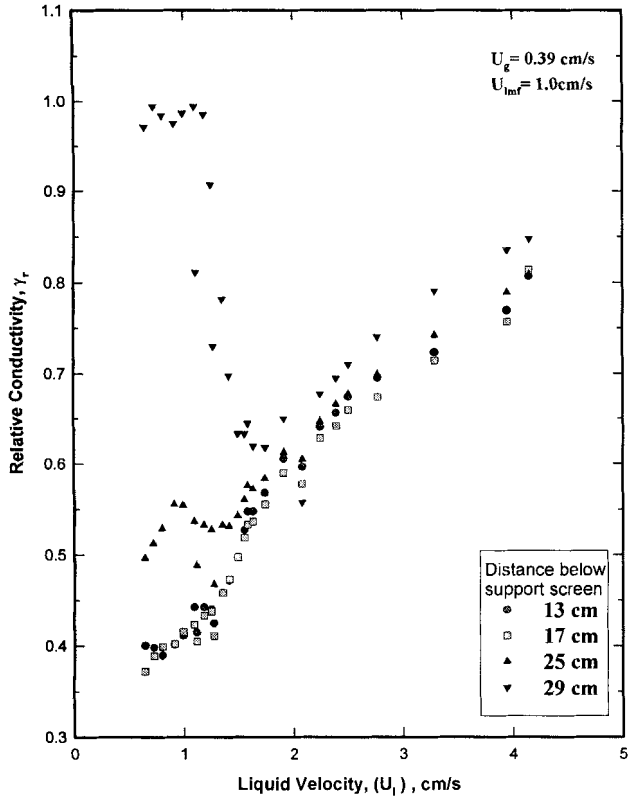

Figure 8. Relative conductivity of the three-phase mixture vs. liquid velocity at different distances z below the support screen (6-mm particles).

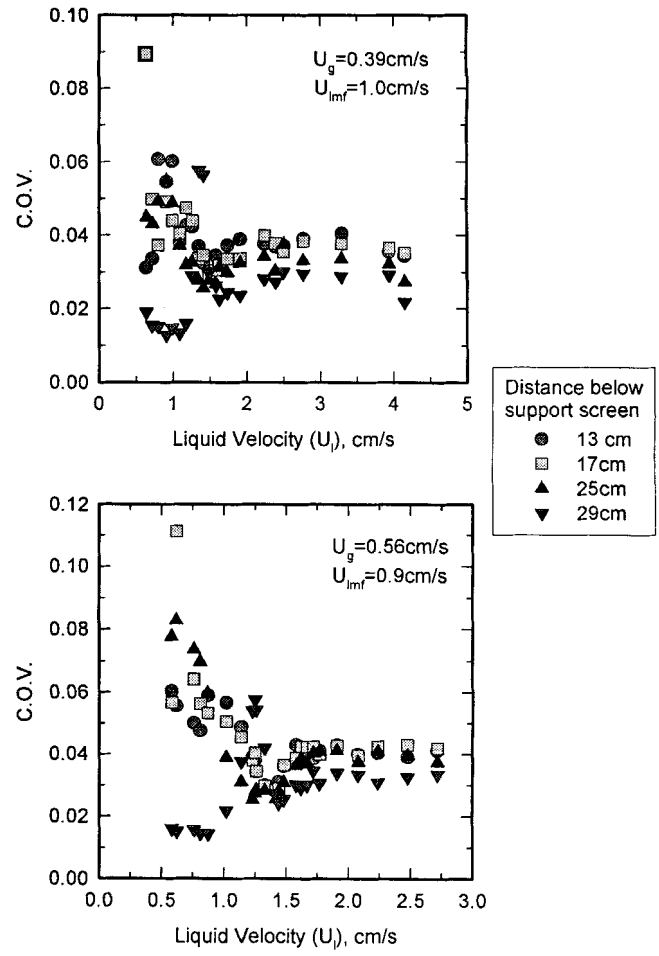

Figure 9. Coefficient of variation (COV) of the signal vs. liquid velocity at different distances below the support screen (6-mm particles).

at any velocity larger than U_{luf}, the fluidization quality and specifically the liquid holdup should be the same everywhere in the bed.

More evidence of the existence of such a uniform fluidization velocity can be obtained by examining the coefficient of variation (COV) of the fluctuations of the conductivity signal. A small COV shows that the fluidization is smooth. Figure 9 shows the variation of the COV with the liquid velocity for two superficial gas velocities, $U_g = 0.39$ cm/s and 0.56 cm/s. The COV decreases when the liquid velocity is increased, and it stabilizes at about the value of U_{luf}, 1.5 cm/s for $U_g = 0.39$ cm/s and 1.4 cm/s for $U_g = 0.56$ cm/s.

These measurements led to the flow regime map shown in Figure 10 for 6 mm particles. Consider what happens when the gas velocity is increased at constant liquid velocity such as 1.0 cm/s, as in Figure 10. At low gas velocity, the bed is fixed. As the gas velocity is increased, the bed progressively fluidizes, starting from the bed surface upward till the U_{lmf} curve is crossed at 0.39 cm/s and the whole bed becomes fluidized. With further increases in gas velocity, the bed expands and some channeling is observed. As the gas velocity is increased and the U_{luf} curve is reached, the bed becomes uniformly fluidized. Figure 11 shows the same hydrodynamic regimes for the 4-mm particles.

Prediction of various phase holdups

As indicated earlier, Legile et al. (1988) and Fan et al. (1982a,b) evaluated the individual phase holdups using the estimated bed height and pressure gradient as follows:

$$-\frac{dP}{dz} = (\rho_l \epsilon_l + \rho_s \epsilon_s + \rho_g \epsilon_g) g \tag{3}$$

$$\epsilon_s = \frac{W}{\rho_s A H} \tag{4}$$

$$\epsilon_l + \epsilon_s + \epsilon_g = 1 \tag{5}$$

The preceding equations implicitly assume that the solid entrainment into the freebroad is negligible. At high gas velocities, however, a lot of solids are entrained into the freeboard and the assumption of a constant solid holdup in the bed, implicit in Eq. 4, is no longer valid. In addition, in solving Eq. 3, *dP/dz* is assumed to be constant, which may not always be the case.

To avoid the problem associated with solids entrainment, the vertical profile of the liquid holdup was obtained instead using conductivity results. This allows for an additional equation that describes the vertical variation of the measured liquid holdup

$$\epsilon_{l\text{calc}} = \epsilon_{lf} + \frac{\epsilon_{ld} - \epsilon_{lf}}{f(z)} \tag{6}$$

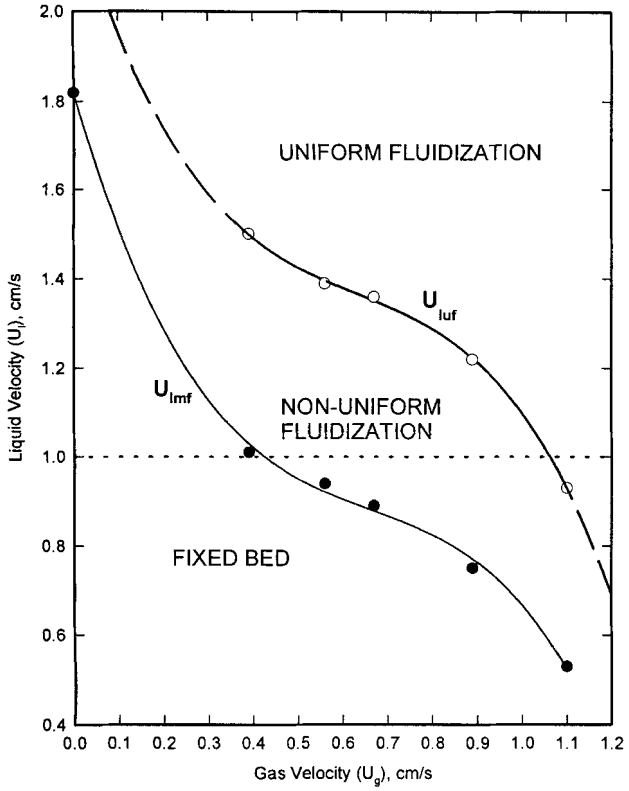

Figure 10. Hydrodynamic regimes in three-phase inverse fluidization (6-mm particles).

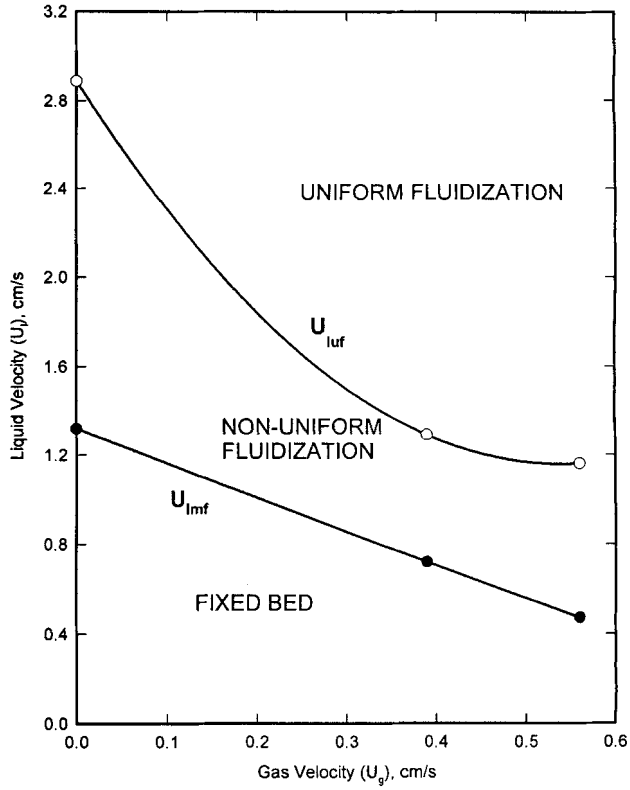

Figure 11. Hydrodynamic regimes in three-phase inverse fluidization (4-mm particles).

where $f(z)$ is a transition function which is equal to one for $z = 0$ and zero for $z = \infty$. The form of $f(z)$ used in this study can be found in the Appendix.

Rearranging Eq. 3 and neglecting the term $\epsilon_g \rho_g$, the local solid holdup can be obtained from the local pressure gradient and the local liquid holdup as follows:

$$\epsilon_s = \frac{1}{\rho_s}\left(\frac{1}{g}\frac{dP}{dz} - \epsilon_l \rho_l\right) \tag{7}$$

which can be used to perform a mass balance on the solids inside the column,

$$W_{\text{calc}} = \int_0^{H_c} \rho_s A \epsilon_s dz \tag{8}$$

Detailed Procedure to get the Phase Holdups.

- Both ϵ_{ld} and ϵ_{lf} are obtained from the experimental values of the relative conductivity (γ_r) in the dense phase and in the freeboard using Eq. 2.
- The variation of the pressure gradient dP/dz with z is obtained by fitting the measured static pressure profile and getting the first derivative. The function used in this study to describe the variation of dP/dz with z is shown in the Appendix.
- The values of the parameters used in the transition function $f(z)$ are then obtained by minimizing the sum

$$S = \left(\frac{(W_{\text{calc}} - W)}{W}\right)^2 + \frac{1}{n}\sum_0^n \left(\frac{(\epsilon_{l\text{calc}} - \epsilon_{l\text{exp}})}{\epsilon_{l\text{exp}}}\right)^2 \tag{9}$$

where $\epsilon_{l\text{calc}}$ is obtained from Eq. 6, W_{calc} is obtained from Eq. 8, and W is the actual mass of solids loaded into the column.

- ϵ_g can then be calculated from;

$$\epsilon_g = 1 - \epsilon_l - \epsilon_s \tag{10}$$

- Finally, the static pressure difference (*relative to the screen level*) is then calculated and compared to the experimental values:

$$\Delta P = \int_0^z g(\rho_l \epsilon_l + \rho_s \epsilon_s + \rho_g \epsilon_g) dz \tag{11}$$

Figure 12 shows conformity of the calculated pressure ΔP, relative to the screen level, to the experimental values for the 6-mm particles. The predicted phase holdup profiles for this particular hydrodynamic condition are depicted in Figure 13. Similar results are presented for the 4-mm particles in Figures 14 and 15. Figures 13 and 15 show that the liquid holdup increases gradually from the bed to the freeboard over a wide transition region. Similarly the solid holdup decreases from the bed into the freeboard. Note that the solid holdup profiles shown in Figures 13 and 15 demonstrate that the assumption of a sharp transition between the bed and the freeboard is not justified. The gas holdup as shown in both figures exhibits a maximum near the bed height estimated from the solid holdup profile, as shown in Figure 13. This high gas holdup value is possibly due to the slowing down of the bub-

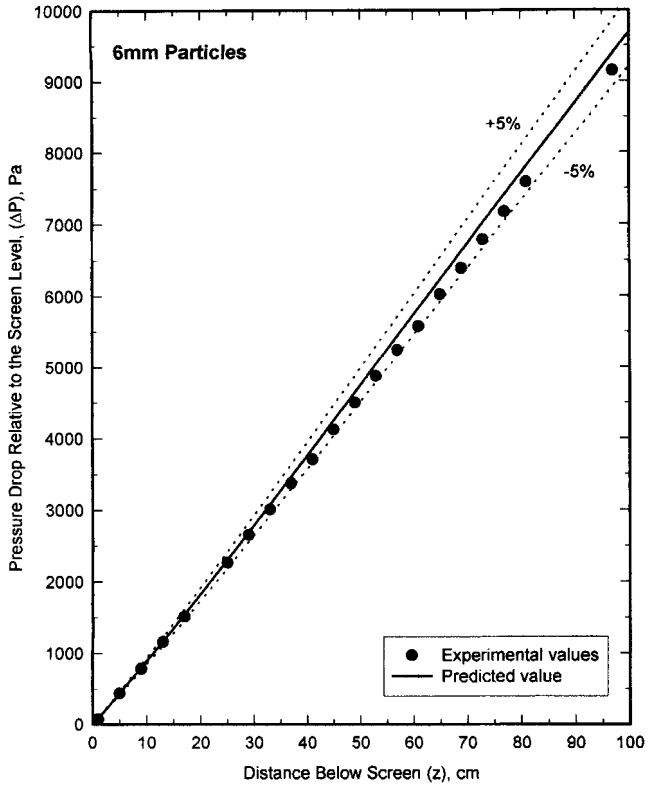

Figure 12. Axial profile of the static pressure.

$U_g = 0.89$ cm/s, $U_l = 1.1$ cm/s, 6-mm particles.

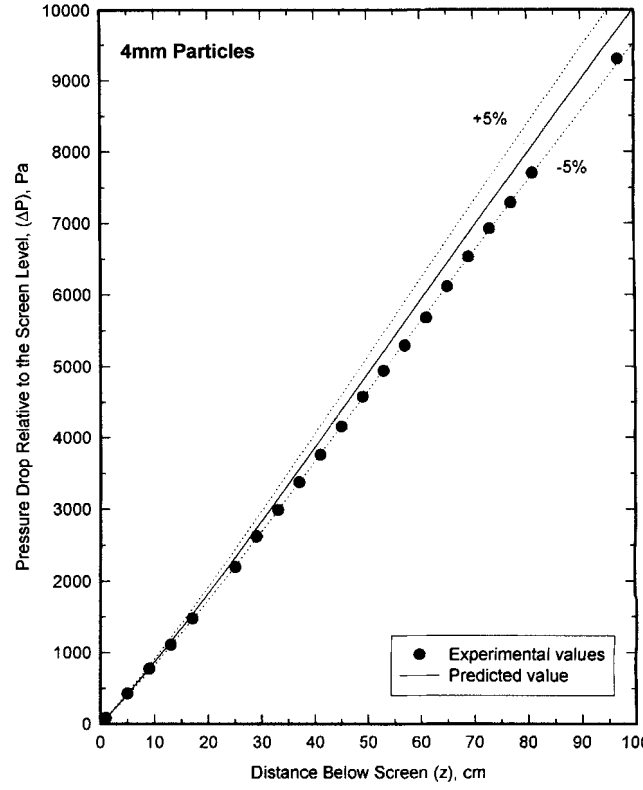

Figure 14. Axial profile of the static pressure.

$U_g = 0.35$ cm/s, $U_l = 0.7$ cm/s, 4-mm particles.

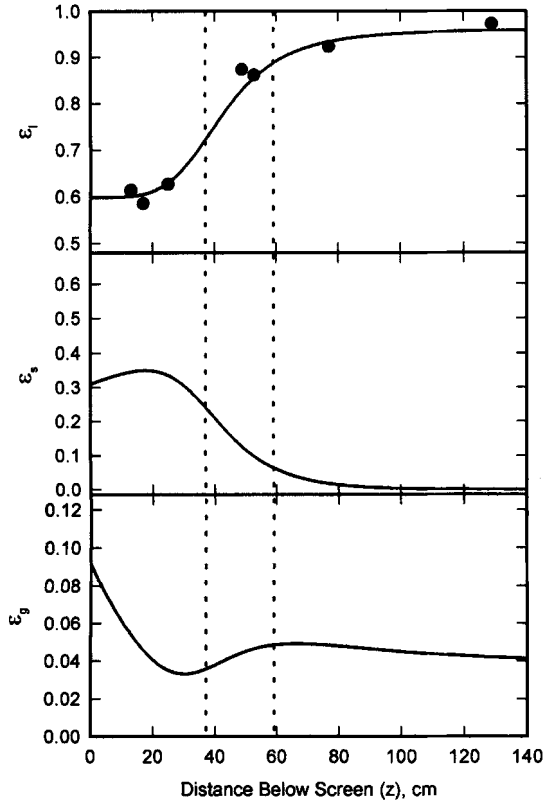

Figure 13. Axial profile of various phase holdups in three-phase inverse fluidization.

$U_g = 0.89$ cm/s, $U_l = 1.1$ cm/s, 6-mm particles.

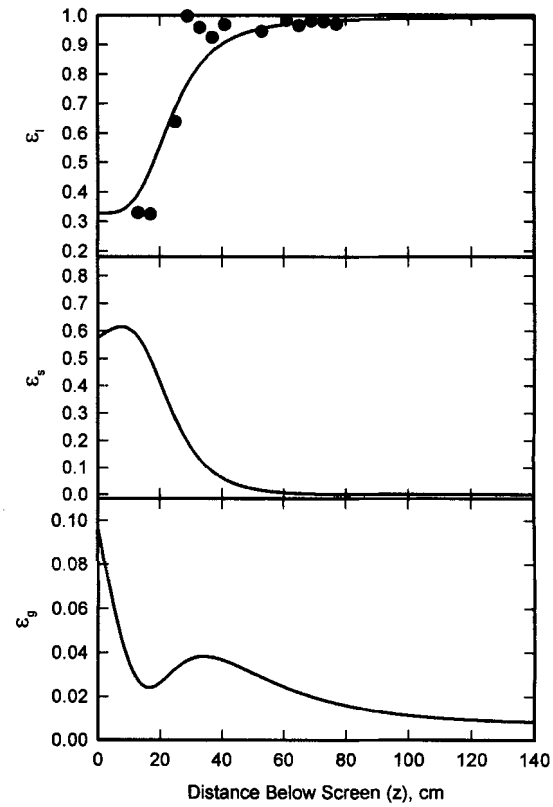

Figure 15. Axial profile of various phase holdups in three-phase inverse fluidization.

$U_g = 0.35$ cm/s, $U_l = 0.7$ cm/s, 4-mm particles.

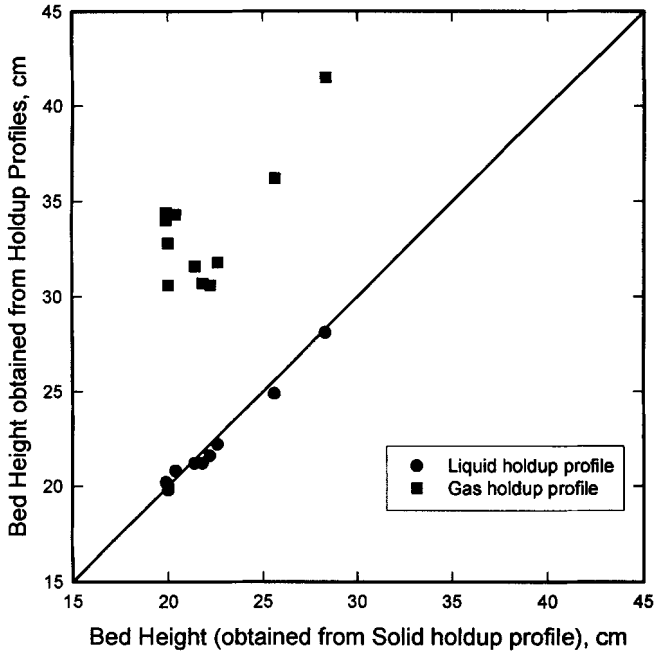

Figure 16. Comparison between the various estimates of the fluidized-bed height (4-mm particles).

bles as they enter the bed. The bubbles will momentarily accumulate and coalesce till the buoyancy of the resulting bubble becomes high enough to push it through the surface. The same phenomenon also occurs near the retaining screen, and these gas bubbles displace some of the particles, resulting in a smaller solid holdup near the screen.

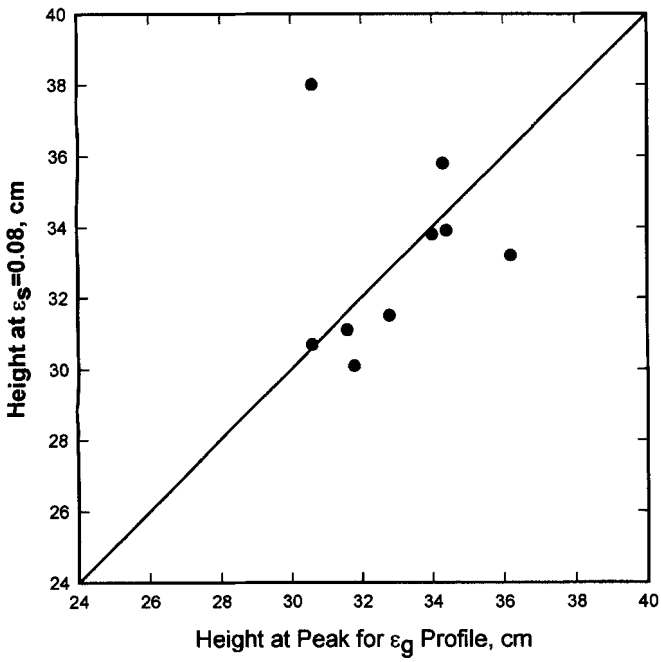

Figure 17. Relation between the height of the gas holdup (ϵ_g) at the peak and the height at solid holdup (ϵ_s) of 0.08 (4-mm particles).

Bed height

In industrial fluidized-bed reactors, it is important to find the fluidized-bed height accurately. Examples of the importance of bed height in design are the positioning of the heat-transfer equipment and the solids withdrawal pipes. In these reactors, often one technique at best can be used to find the bed height while operating. From a theoretical point of view, the bed is characterized by the presence of particles and the freeboard by the absence of particles. Accordingly, the height at which the solids holdup shows a maximum variation is often taken as the bed height. From a practical point of view, this definition of bed height is often the most relevant. The different techniques used in this study for determining the bed height will be discussed in the following section.

In this study, two independent measuring techniques were used to find the phase holdup vertical profiles. In Figure 13, it can be seen that the bed height can be independently obtained from the various phase holdup profiles. The bed height was obtained at the inflection point for both the liquid and

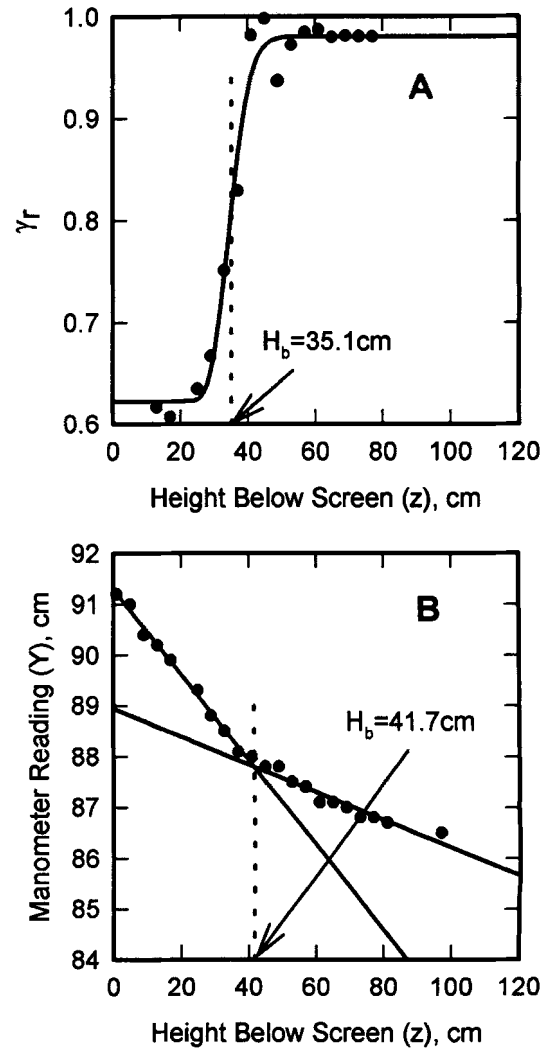

Figure 18. Prediction of bed height: (A) conductivity, (B) static pressure measurements.

U_g = 0.35 cm/s, U_l = 1.5 cm/s, 4-mm particles.

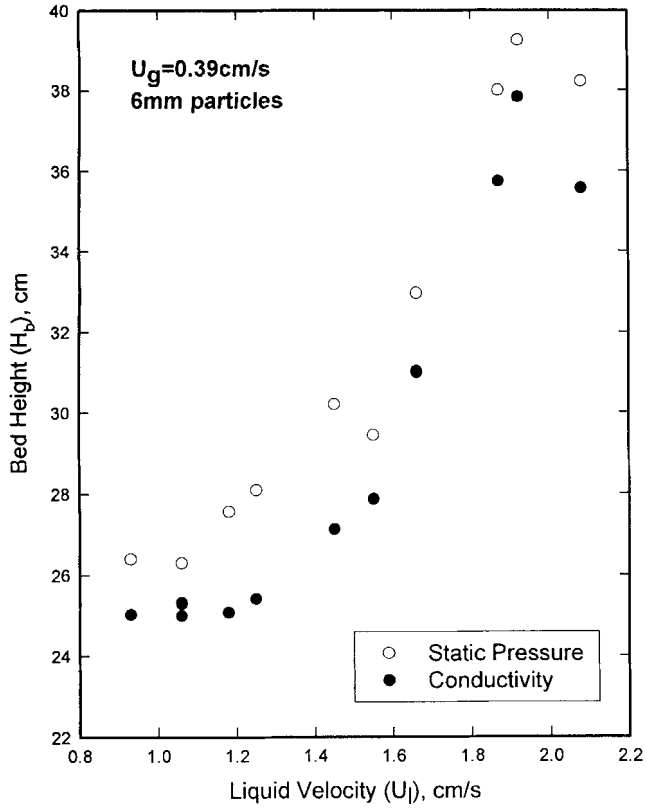

Figure 19. Bed height (obtained from conductivity and static pressure measurements) vs. liquid velocity (6-mm particles).

the solid holdup profiles and at the peak of the gas holdup profile. The different values obtained are shown in Figure 16. It can be seen that the bed height obtained from the solid holdup profile and that obtained from the liquid holdup profile are in nearly perfect agreement. However, the bed height obtained from the gas holdup profile is always higher.

Visual observation indicated that the bubbles tend to accumulate below the bed surface where enough solids are present to slow their motion. Figure 17 suggests that the bed will offer enough resistance to the flow of the bubbles at a solid holdup of about 0.08.

As shown earlier, the bed height predicted from the liquid holdup profile and the solid holdup profile agree well, while the one obtained from the gas holdup does not. This finding is very important when selecting a technique to measure the bed height. Techniques that are based on measuring the gas holdup, for example, gas radioactive tracers or bubble probes, may not give accurate results, since the height obtained will be the height as seen in Figure 16. On the other hand, any technique that provides the bed height from either the liquid holdup or the solid holdup profiles would be suitable. For bed heights based on the liquid holdup profile, radioactive tracers and conductivity can be used. Solid radioactive tracer technique would give the bed height based on the solid holdup profile.

Other techniques—γ rays, static pressure measurements, and capacitance—will give the bed height based on the density of the three-phase mixture. When the density of the solid particles is close to that of the liquid, the bed height obtained by such methods will be affected mainly by the gas holdup. Therefore, it is very important to compare the bed height based on the solid holdup or the liquid holdup (conductivity) to that based on the density of the mixture (static pressure). Figure 18 shows the variation of relative conductivity and manometer reading with height for a typical experiment. The bed height can be found from conductivity data by assuming it is located at the inflection point, for example, 35.1 cm in Figure 18a. The standard technique is to obtain the bed height from the vertical pressure profile (Fan et al., 1982a; Legile et al., 1988). The bed height is then assumed to be at the intersection of the two straight lines representing the bed and the freeboard, for example, 41.7 cm in Figure 18b.

Figures 19 and 20 show that the bed height predicted by the conductivity method is smaller than the one predicted by the static pressure method. Since the liquid is the only conductive phase, the conductivity method measures the height at which the liquid holdup is half-way between the liquid holdup in the bed and in the freeboard. The static pressure method measures the height at which the density of the gas–liquid–solid mixture, in the column, is half-way between its values in the bed and in the freeboard. The bed height measured by the static-pressure method was higher than that measured by conductivity, for both particle sizes as shown in Figures 21 and 22. It can be seen that for 95% of all hydrodynamic conditions, the bed height from static pressure is higher by 15% for the 6-mm particles and 30% for the 4-mm particles. The 4-mm particles have less mass and inertia than the 6-mm particles, giving a wider transition.

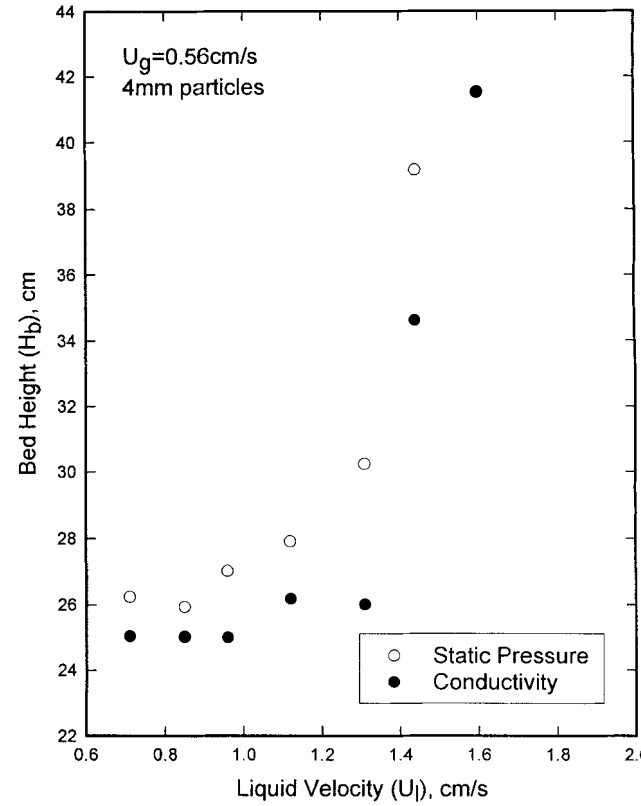

Figure 20. Bed height (obtained from conductivity and static pressure measurements) vs. liquid velocity.

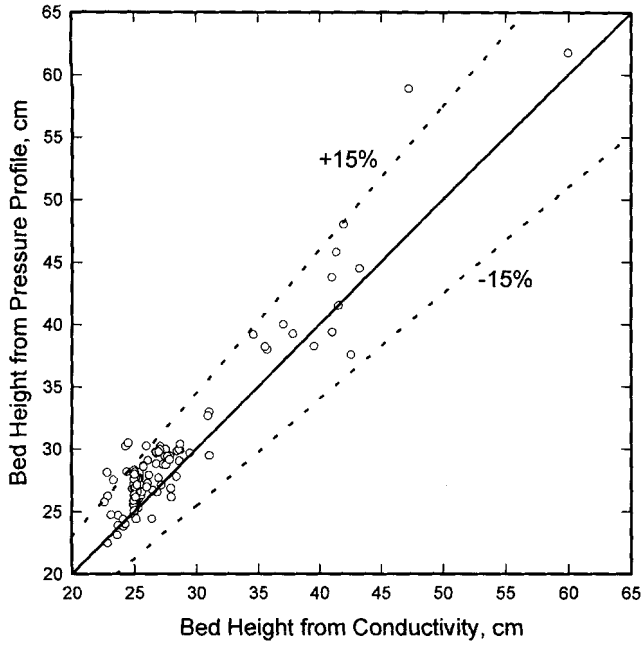

Figure 21. Bed height obtained from static pressure vs. bed height obtained from conductivity.

Gas–liquid–solid system, 6-mm particles.

In this study, it was decided to use both static pressure and conductivity methods to determine the bed height since they provide distinct and useful information. The data for the bed height were correlated with the liquid velocity and the gas velocity. Figure 23 shows a three-dimensional plot for the bed height (conductivity) as a function of U_g and U_l, and Figure 24 shows the same plot for the bed height obtained from the static-pressure method.

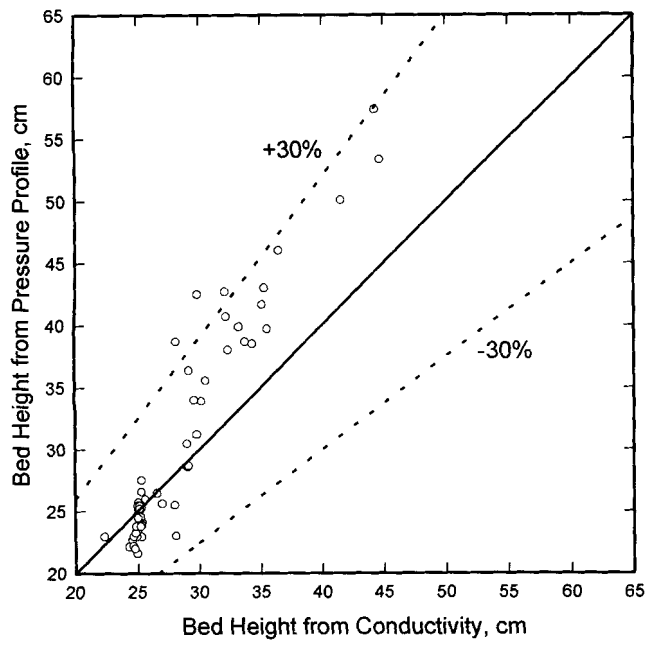

Figure 22. Bed height obtained from static pressure vs. bed height obtained from conductivity.

Gas–liquid–solid system, 4-mm particles.

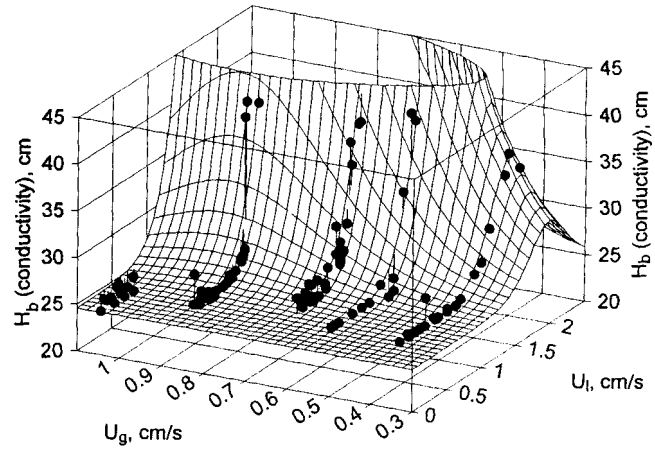

Figure 23. Three-dimensional plot of the bed height (obtained from conductivity measurements) vs. liquid and gas velocities (6-mm particles).

Figure 25 shows that the expanded bed height obtained from the conductivity method increased as either the liquid velocity or the gas velocity was increased. The same fluidized bed height can be obtained either at a low gas velocity and a high liquid velocity or at a higher gas velocity and a lower liquid velocity. This finding was also reported by previous researchers (Fan et al., 1982a,b; Legile et al., 1988). At higher gas velocities, the bed height increases more rapidly as the liquid velocity is increased. The gas displaces some of the liquid, reducing the liquid holdup and thus increasing the interstitial liquid velocity (U_l/ϵ_l). This increases the drag exerted on the particles by the liquid and hence the bed expansion.

Conclusions

When measuring the bed height in three-phase fluidized beds that display a significant transition zone, the obtained bed height depends on the measuring technique. For example, static pressure and conductivity measurements may give

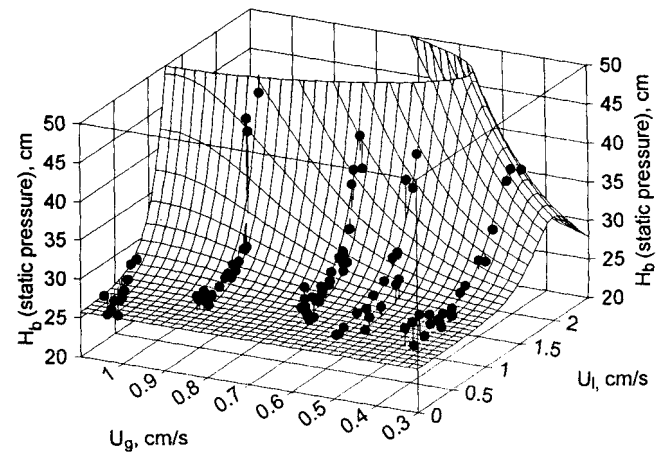

Figure 24. Three-dimensional plot of the bed height (obtained from static pressure measurements) vs. liquid and gas velocities (6-mm particles).

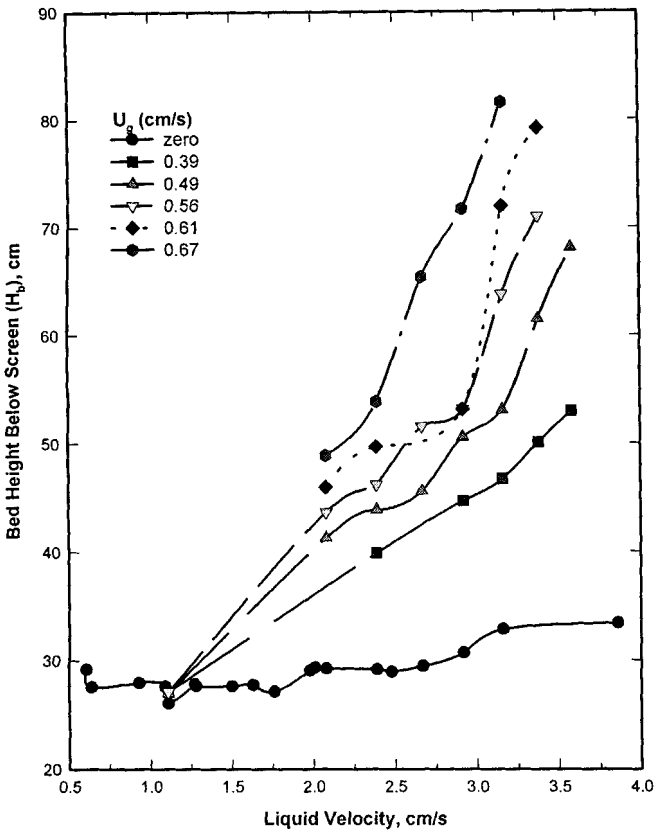

Figure 25. Bed height (obtained from conductivity measurements) vs. liquid velocity at constant gas velocity (6-mm particles).

bed heights that differ by up to 30%. To get a complete picture, two independent measurement methods are required. In this study, static pressure and conductivity measurements were combined to obtain the vertical gas, liquid, and some holdup profiles.

The minimum liquid fluidization velocity was obtained from the bed static-pressure gradient. It was found to decrease as either the liquid velocity or the gas velocity was increased.

A new transition velocity, called the uniform fluidization velocity, was identified using conductivity measurements. This is the superficial liquid velocity at which the fluidization quality becomes the same throughout the bed.

Acknowledgments

A research grant from the Natural Sciences and Engineering Research Council of Canada to Dr. M. A. Bergougnou made this work possible. It is most gratefully acknowledged. Dr. L. S. Fan, Ohio State University, lent us a batch of polypropylene particles. His help is greatly appreciated.

Notation

A = cross-sectional area of the column, m^2
D_c = inside diameter of the column, m
d_p = particle diameter, m
g = gravitational acceleration, 9.81 m/s^2
H = total height of the fluidized bed, m
H_b = height of fluidized bed, m
H_c = height of the column, m
S = error term defined in Eq. 8
U_{lmf} = minimum liquid fluidization velocity as obtained from pressure measurements, m/s
Y = manometer reading, cm
z = height below the screen, m
z_l = adjustable parameter for liquid holdup transition function, $f(z)$, m
α_l = adjustable parameter for liquid holdup transition function, $f(z)$
ϵ_{ld} = liquid holdup in the dense phase
ϵ_{lf} = liquid holdup in the freeboard
Γ_0 = conductance with liquid only
γ = conductivity of a gas–liquid–solid mixture
γ_0 = conductivity of liquid only

Literature Cited

Begovich, J. M., and J. S. Watson, "An Electroconductivity Technique for the Measurement of Axial Variation of Holdups in Three-Phase Fluidized Beds," *AIChE J.*, **24**(2), 351 (1978).

Chern, S.-H., "Hydrodynamic Characteristics of Liquid-Solid and Gas-Liquid-Solid Fluidized Beds," PhD Thesis, The Ohio State Univ., Columbus (1982).

Chern, S.-H., K. Muroyama, and L.-S. Fan, "Hydrodynamics of Constrained Inverse Fluidization and Semifluidization in a Gas-Liquid-Solid System," *Chem. Eng. Sci.*, **38**(8), 1167 (1983).

Fan, L.-S., K. Muroyama, and S.-H. Chern, "Hydrodynamic Characteristics of Inverse Fluidization in Liquid-Solid and Gas-Liquid-Solid Systems," *Chem. Eng. J.*, **24**, 143 (1982a).

Fan, L.-S., K. Muroyama, and S.-H. Chern, "Some Remarks on Hydrodynamics of Inverse Gas-Liquid-Solid Fluidization," *Chem. Eng. Sci.*, **37**(10), 1570 (1982b).

Fan, L. S., *Gas-Liquid-Solid Fluidization Engineering*, Butterworth, Stoneham, MA (1989).

Karamanev, D. G., and L. N. Nikolov, "Bed Expansion of Liquid-Solid Inverse Fluidization," *AIChE J.*, **38**(12), 1916 (1992).

Legile, P., G. Menard, C. Laurent, D. Thomas, and A. Bernis, "Contribution a l'etude hydrodynamique d'un lit fluidise triphasique inverse fonctionnant a contre-courant," Entropie No. (143–144), 23 (1988). (Translated as "Contribution to the Study of an Inverse Three-Phase Fluidized Bed Operating Countercurrently," *Int. Chem. Eng.*, **32**(1), 41 (1992).)

Page, R. E., "Some Aspects of Three-Phase Fluidization," PhD Thesis, Univ. of Cambridge, Cambridge, England, p. 137 (1970).

Shimodaira, C., Y. Yushina, H. Kamata, H. Komatsu, A. Kurima, O. Mabu, and Y. Tanaka, "Method and Apparatus for the Biological Treatment of Wastewater," U.S. Patent 4,256,573 (1981).

Thomas, D., and A. Bernis, "Incidence de l'aptitude a la coalescence du fluide sur l'hydrodynamique d'un lit fluidise triphasique inverse fonctionnant a contre-courant," *Recents Progres en Genie des Procedes*, Vol. 3 (8a), Toulouse, France, p. 161 (1989).

Appendix

The transition function $f(z)$ used in Eq. 6 is

$$f(z) = 1 + \left(\frac{z}{z_l}\right)^{\alpha_l}.$$

The continuous function used to describe dP/dz vs. z is

$$\frac{dP}{dz} = \left(\epsilon_{lf} - C_l \exp\left(\frac{-z}{C_2}\right)\right)\rho_l g,$$

where C_1 and C_2 are constant and are obtained by regression from the pressure profile.

Manuscript received July 10, 1995, and revision received Nov. 16, 1995.